DC Collection Network Simulation for Offshore Wind Farms

Vogel, Stephan; Rasmussen, Tonny Wederberg; El-Khatib, Walid Ziad; Holbøll, Joachim

Published in:
Proceedings of EWEA Offshore 2015 Conference

Publication date:
2015

Document Version
Publisher's PDF, also known as Version of record

DC Collection Network Simulation for Offshore Wind Farms

(EWEA Offshore 2015, Copenhagen, Denmark)

Stephan Vogel*, Tonny Wederberg Rasmussen†, Walid Ziad El-Khatib‡ and, Joachim Holbøll‡
Technical University of Denmark
Richard Petersens Plads, Building 325, 2800 Kongens Lyngby
Email: stevog@elektro.dtu.dk*, twr@elektro.dtu.dk†, wzel@elektro.dtu.dk‡, jh@elektro.dtu.dk§

***Abstract*—The possibility to connect offshore wind turbines with a collection network based on Direct Current (DC), instead of Alternating Current (AC), gained attention in the scientific and industrial environment. There are many promising properties of DC components that could be beneficial such as: smaller dimensions, less weight, fewer conductors, no reactive power considerations, and less overall losses due to the absence of proximity and skin effects.**
This work describes a study about the simulation of a Medium Voltage DC (MVDC) grid in an offshore wind farm. Suitable converter concepts are identified and the power flow in steady-state and during fault conditions is investigated. The efficiency of the network is determined in full-load conditions. Furthermore, key design aspects of such a grid are illustrated and issues regarding ripple current and converter design are treated. The overall efficiency of the MVDC grid is determined to 94%.

I. Introduction

The possibility to use a DC-collection grid instead of AC-collection grid inside an offshore wind farm was introduced in several scientific reports in recent years [1] [2] [3] [4]. Benefits, like material and weight savings in cables and transformers are paired with a general higher efficiency, enabling this technology to become superior in the future. Since an efficient transmission of current requires a voltage above the state of the art generator voltage of $0.69kVAC$ $(1kVDC)$, the internal collection grid voltage needs to be boosted to a medium voltage. DC/DC converters enable this process in a DC grid, and different topologies are suggested such as the Dual-Active Bridge converter (DAB) [5] and the Bi-directional Thyristor Converter (BTC) [6]. However, market information about the development progress of these innovative converters are hard to find (Status: 06/2014). Furthermore, some main challenges are identified when DC collection grids are considered. Since DC currents naturally do not cross the zero current mark in time, they are more difficult to disrupt during fault conditions. Special breakers need to be implemented that are able to break the high DC currents and market availability of those switches needs to be established. Secondly, the lack of field experience leads avoidance by many wind farm developers. Without experience, the first applicant of a new technology has to deal with start-up problems that might be expensive. Thirdly, the lack of standardisation for DC grids hampers the development of the components. Therefore, further research about the various system configuration needs to be performed and documented. This paper provides information about the operability of DC-collection girds for offshore wind farms. At first, the reader is introduced to an overview of such a grid and the basic properties are highlighted. Afterwards, a detailed study regarding the necessary components of this network are determined and key aspects like principle of operation and control of the component are elaborated. Then, all electrical models are implemented in the grid simulation transient simulation program PSCAD/EMTDC and the steady-state power flow is simulated. Additionally, the grid was exposed to transient short-circuit events and while the voltages and currents are monitored. To conclude, the efficiency of the DC-grid is determined by calculation of the conduction and switching losses in the components.

II. DC Collection Grid Overview

In Figure 1, an offshore wind farm is illustrated which operates with a DC grid configuration. The 0.69 kV AC synchronous generator output is rectified with a passive AC/DC diode bridge. Capacitive filters operate in parallel to stabilize the voltage in the event of a transient voltage. The output of the diode rectifier is boosted with a DC/DC converter system up to 30 kV. This medium voltage is chosen to compare the losses with the existing 33 kV AC grids. The power is collected in the DC collection network and transmitted to the HVDC-platform, where the voltage is further stepped-up to 300 kV. On land, the HVDC/AC inverter transforms the DC current to AC and injects it into the local grid. The grid codes for the wind farm apply at the Point of Common Coupling (PCC) and need to be controlled by the HVDC/AC inverter.
The orange arrows in Figure 1 indicate the control responsibilities of the single converter blocks. The low voltage is controlled by the DC/DC wind turbine converter, whereas the DC grid voltage is maintained from the HVDC boost-converter. Several connection strategies for offshore wind farms are reviewed. In this work, a parallel MVDC grid layout is used due to the robust design and the controllability. The maximum transmitted power through a cable is given by the location in the bus and the output power of the turbine. Another possibility to connect an offshore wind farm is a series connection with several parallel feeders. In this concept, the wind turbines boost the voltage directly up to transmission voltage and no additional HVDC boost converter is necessary. The main drawback of such a system is the vulnerability of the grid to faults and the necessity to overate wind turbine DC/DC converters. A surround investigation regarding connection concepts of offshore wind farms is performed in [7].
Following benefits and challenges of direct current collection grids should be highlighted:

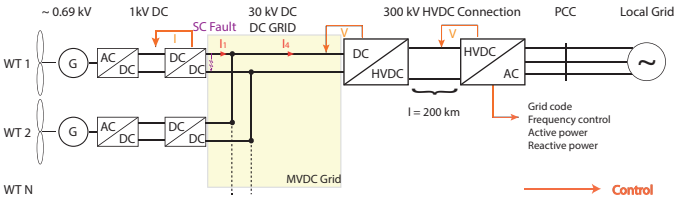

Fig. 1: Overview of MVDC grid with main components, voltage levels and control responsibilities

Advantages:

- No heavy 50 Hz transformer in the turbine necessary
- No contribution of reactive power in the grid
- 2 phases instead of 3 phases
- No skin and proximity effects - only resistive losses in the cables
- DC/DC converters can have modular structure
- DC/DC conversion with medium frequency decreases component size

Challenges:

- Technology is untested for large scale MW application
- No DC-standards - regulation essential
- Challenges arise with medium frequency transformers
- Fast DC-breaker to limit short-circuit currents are essential

III. Electrical Component Models

This section aims to find appropriate electrical representations to describe the behaviour of the MVDC-grid.

A. Wind Turbine Model with AC/DC Rectifier

In this study, a four-pole synchronous generator is used to provide the electrical conversion of torque to electric power. The drive train, rotor and wind turbulence is not a part of the simulation, since it extends the simulation time drastically. Furthermore, the transient response of mechanical systems is composed of higher time constants compared to the fast time constants of electrical systems. Therefore, it is valid to neglect this representation for short time intervals. The generator model is presented in Figure 2. It consists of synchronous machine with rated power S = 5 MVA and an exciter model. Both models are utilized from the PSCAD model library. The torque of the machine can be adjusted by a slider and is set to 1 pu during the simulation. Since the machine does not synchronize with a grid, the rotational speed of the machine can vary. This is a necessary feature for a variable speed wind turbine. The output of the machine is connected to a standard diode bridge rectifier. No active power conversion components are necessary.

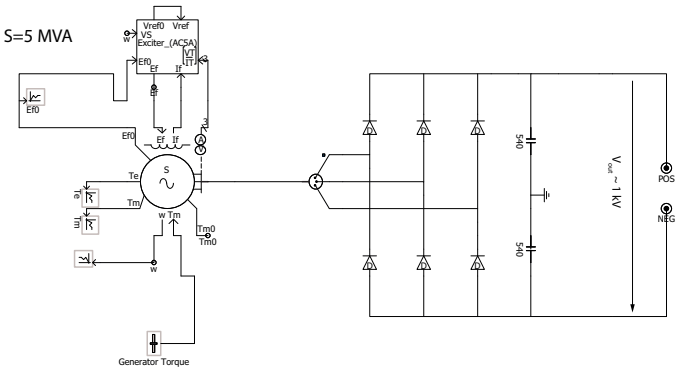

Fig. 2: Generator and Diode Rectifier

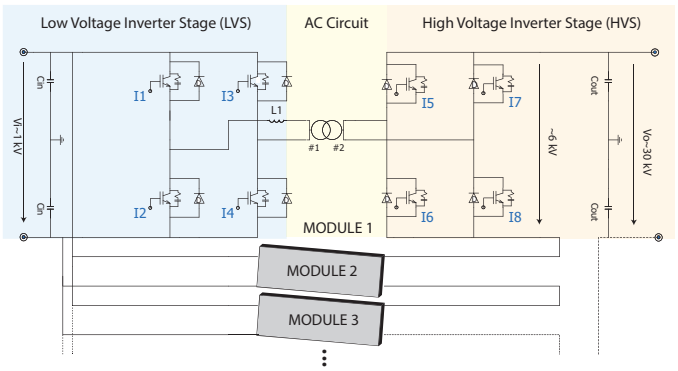

Fig. 3: Parallel Dual-Active Bridge Design

B. DC/DC Step-up converter

The purpose of a DC/DC converter is to step-up the voltage. This is necessary to decrease transmission losses in the cables and conduction losses in the converter. The DC/DC converter requirements for the MVDC are listed below:

- Voltage step-up ratio from 1 kV to 30 kV
- High-power transmission capability up to several MW
- Bi-directional power flow
- The losses of the converter and the estimated costs for the components are reasonable

1) Dual-Active Bridge (DAB)- Topology: The DAB converter, first proposed in [5], is a high power density, low loss and easy to control DC/DC converter. The converter is able to be operated bidirectionally, in step-down or step-up voltage mode. In Figure 3, the main topology is illustrated. The converter consists of two active full bridges interconnected via a small and light medium-frequency transformer. Furthermore, an inductor is essential in the AC circuit of the topology that may be inherent in the transformer reactances. The active power flow is controlled by varying the phase shift displacement between the two bridges via the inductance. The two bridges operate with two-level square wave switching. This provides the converter with a significantly speed increase compared to pulse-width modulated control strategies, since no sine wave is modulated. There are three reasons to divide the converter structure into several modules. Firstly, the power

level of a 5 MVA wind turbine forces very high currents through the low voltage inverter stage, since the input DC voltage of the DAB converter is set to 1 kV. After the first design of the DAB was tested with just one module, the concept was withdrawn due to the high conduction losses in the switches. The second simulated approach used a modular design with a parallel input connection on the Low Voltage Stage (LVS) and a series connection of the modules on the High Voltage Stage (HVS). With this design, the currents on the LVS and the voltage on the HVS are divided by N number of modules. The second benefit from a modular converter structure is the scalability and replaceability. Other power ratings can easily be achieved for other wind turbine sizes and, in case of a failure, a module of a converter is easier to replace than the whole converter. The third advantage relates to the medium frequency transformer design. Since the HVS is connected in series, the step-up voltage is shared among the modules. Therefore, one module does not need to span the full voltage ratio of $1kV/30kV$, but the module output voltage is divided by N stages.

$$V_m = \frac{V_2}{V_1} = \frac{30kV}{1kV\,N} \tag{1}$$

This enables an improved transformer design as shown in [8]. One crucial part of the DAB converter is the the medium-frequency, high-power transformer. It enables the converter to step-up/down the voltage and provides galvanic isolation between the LVS and HVS. Compared to normal 50/60 Hz transformers, the size of a medium frequency transformer in a DAB converter is significantly decreased due to the dependency of the magnetic core cross sectional area A_c to the frequency.

$$A_c = \frac{V_{rms1}}{\sqrt{2}\pi f B N_1} \tag{2}$$

where V_{rms1} is the root mean square value of the primary voltage, B_p is the peak flux density, N_1 is the number of primary turns, and f is the frequency. The magnetic core dimensions can be decreased with increased operational frequency, and still the rated power can be applied. Increasing the operation frequency causes skin, proximity, hysteresis, and dielectric losses to be increased significantly. Therefore, a careful investigation of the temperature distribution in the transformer has to be performed, and new transformer materials need to be considered. More information can be found in [9].

2) Dual-Active Bridge (DAB)- Control: The control of the DAB converter can be executed easily with Single Phase Shift (SPS) between the two bridges [5]. However, this control strategy has some disadvantages regarding reactive power and harmonics. Therefore, the Dual Phase Shift (DPS) control system was implemented [10].

In Figure 4, the control schematic is illustrated. The base of the control is a reference saw tooth signal (X) which is operating at a constant frequency ($f_s = 5kHz$) with a peak value of $\hat{X} = 2\pi$. The switching frequency is limited due to the loss generated in the semiconductor devices. This saw tooth signal is fed into the SinPhi block to generate the reference sine wave for all gate signals. The phase displacement, φ, of the sine wave depends on the output of two separated PI-controllers.

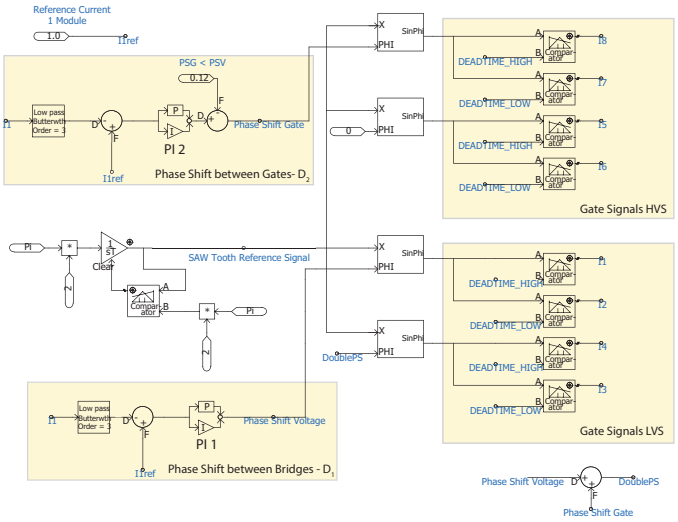

Fig. 4: DAB Control Schematic

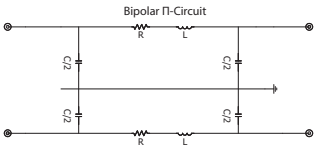

MVDC Cable	
Rated Phase to Ground Voltage [kV]	± 15
Cable Length [km]	0.45
Steady State Current [kA]	4 * 0.166 = 0.664
Cross Sectional Area [mm^2]	500
Line Resistance [Ω/km]	0.0366
Line Inductance [mH/km]	0.357
Parasitic Capacitance [μ F/km]	0.3

Fig. 5: Model Bipolar PI-Circuit

In this control pattern, two separate PI-controllers are used to generate the phase shift between the bridges, D_1, and the phase shift between the gates, D_2. The input for both PI's is the input current I_1 compared to a reference current I_{1ref}. The output of $PI_1 = D_1$ shifts the gate signals from the LVS in relation to the HVS. The output of $PI_2 = D_2$ generates the displacement between the valves I_8/I_7 in relation to I_5/I_6, as well as I_3/I_4 in relation to I_1/I_2. Additionally, the possibility to define dead-times between the gate signals is given to avoid short-circuits in the converter legs.

C. Cable Models

1) MVDC Cable Model: The wind farm internal cabling consists of commercially available medium voltage cables. The distance between wind turbines can be estimated as $450m$ and the distance between the wind turbine feeders as $900m$. In [11], an overview of three different DC cable modelling methods for MVDC/HVDC transmission systems are provided. It is shown that the simplest model, the π-model, can provide results which are as accurate as more complex frequency-dependant phase model for short distances up to 15 km. This statement always depends on the frequency of the fault oscillations. The higher the frequency in the network, the less the π-modelling method is valid. However, due to simulation time, the cable model inside the wind farm is realized with a lumped π-model. The parameters for a MVDC cable are included in Figure5. The values for resistance, inductance, and capacitance depend on the cable type and the diameter of the conductor. The diameter of the conductor, in turn, depends on the maximum conducted current.

2) HVDC Cable Model: Voltages and currents can be seen as travelling waves in cables. They have a finite travelling speed, and their progression along the line may cause reflections and refractions at the end of the line. Those occurrences can further create local peak points of current and voltage; however, the natural resistance of cables damps-out the peak values of the wave. The lumped $\pi - model$ is not able to model the effect of a travelling wave along the line, since the capacity is lumped to the front and end of the line. The model is sufficient to simulate short cable segments inside the wind farm but if the transmission distance increases, another model needs to be introduced.
Fortunately, PSCAD provides several elaborated models to accurately take long distance transient responses into account. For this purpose the "Frequency Depended Phase Model" FD was implemented into the simulation. Frequency depended models are distributed travelling wave models. However, the system resistance R is distributed across the system length (along with L and C) instead of lumped at the end points. More importantly, the frequency depended models are solved at a number of frequency points, thereby including the frequency dependence of the system [12]."
The cable parameters used are chosen by utilization of the cable ratio from [13] and recalculated to a $800mm^2$ cross-section cable. The cable structure consists of six layers: main conductor, insulator 1, sheath, insulator 2, armour and insulator 3.

D. Breakers

The breakers are modelled as perfect switches which are able to break any magnitude of current. They are controlled with a PSCAD logic. More information about the used breaker times can be found in Section IV-B.

E. HVDC Boost Converter

The purpose of the HVDC-boost converter is to raise the internal 30 kV grid voltage to a higher transmission potential of 300 kV. The schematic of the proposed boost converter can be seen in Figure 6. The topology is rather simple and well known from low power boost converters; however, the boost converter concept is scalable and needed power components are readily available on the market. Notice that IGBT and diode needs to withstand the full $\pm$ 150 kV, resulting in a high amount of stacked components. The component dimensioning of the inductor was performed according to [14].

Only unidirectional power flow is possible with the used model. A bi-directional topology could be designed as well, however, the efficiency and costs of such a converter might not be as competitive since, all the components need to be dimensioned for the rated voltage or current, depending on the component location. On the other hand, a separate buck converter can be dimensioned for just the power level the wind farm needs in idle mode. Therefore, the assumption is made that a separate buck converter takes over operation if the wind conditions demand that the wind farm is an electrical consumer and hence, the power direction is reversed. The step down converter is not modelled in this work because the idle mode of the farm is not a case of this project.

Additionally to step-up the voltage, the boost converter controls the internal DC voltage as illustrated in Figure 1.

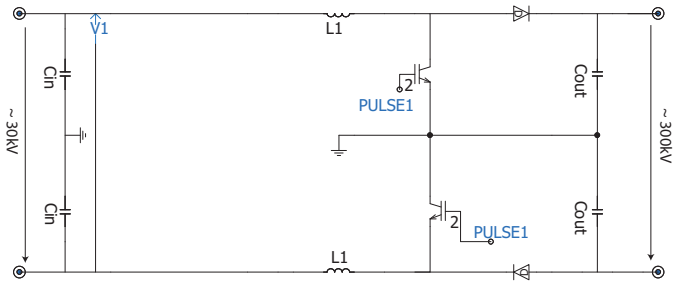

Fig. 6: Boost Converter Schematic

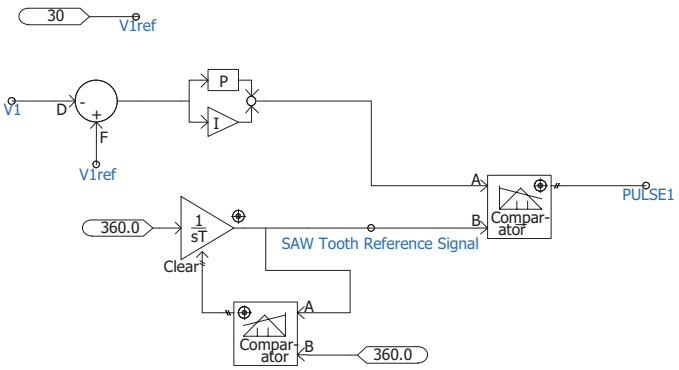

Fig. 7: Control for Boost Converter

A simple voltage regulator structure with a PI-controller was implemented. The control circuit of the structure can be seen in Figure 7.

F. HVDC DC/AC Converter

The HVDC-inverter is the key component to connect the wind farm to the grid on land. The model consists of a two-level IGBT full-bridge inverter Voltage-Source-Converter (VCS) connected via an inductor to a three-phase grid (See Figure 8). By controlling the currents in the inductors, the active and reactive power flow between the inverter and the grid can be controlled. Bidirectional power flow is possible. The converter is controlled with Pulse Width Modulation (PWM) techniques that. Nowadays, HVDC-VSC normally use Modular Multi-level Converter (MMC) structures with have the ability to share the voltage between several sub-modules per valve. The focus on this work, however, is directed to the DC grid and therefore, just the simple two-level model is applied.

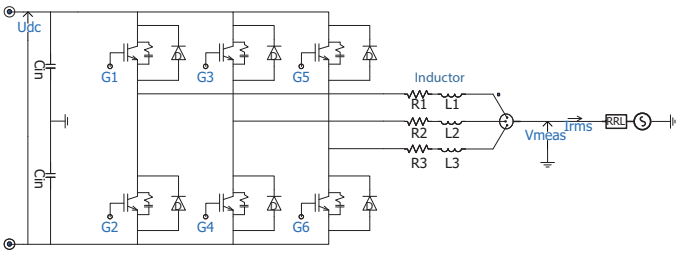

Fig. 8: Schematic for HVDC Inverter

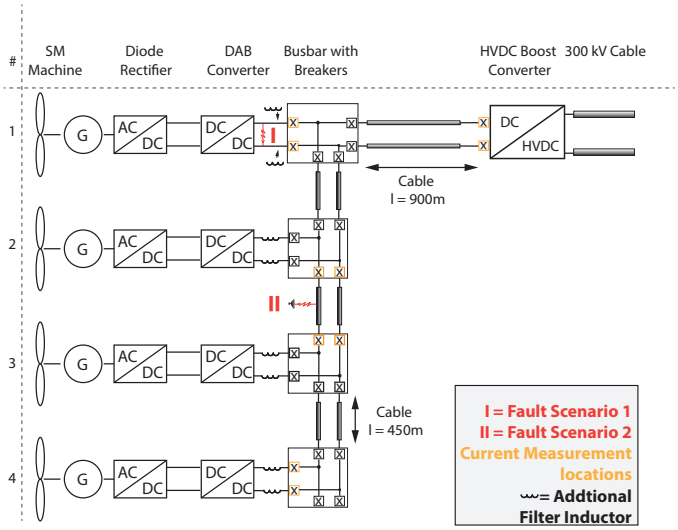

Fig. 9: Grid Overview and Current Measurement Positions for Fault Scenarios

To control the HVDC-inverter, a vector-control structure published in [15] is used. In this paper, the line voltages and currents are transformed into dq0-reference frame, where steady state values appear to be constant. By exploiting this feature, regular PI-controller can be used to independently control active and reactive power with the equivalent currents i_d and i_q.

IV. Grid Simulation

In this section, the overview of the simulated DC-collection grid is introduced. All components from Section III are assembled together to form the network. An illustration of the system is given in Figure 9. The grid consists of four wind turbines which are connected in one DC feeder. Every turbine is protected by DC breakers that are located at the terminal connection points. Additionally, each cable segment between the turbines can be isolated. With this arrangement, in case of a fault, it is possible to exclude the wind turbine or the cable segment while maintaining the operation of the turbines that are not affected. The current is monitored in the breakers and the locations are marked in Figure 9. Due to the complexity of the models and the resulting simulation time, it was only possible to simulate one feeder.

A. Steady state simulation

To approach a meaningful fault analysis, the first step is to investigate the steady state conditions. The purpose is to show currents and voltages in the system and to look for irregularities in the patterns. Figure 10 shows the system in steady state conditions. As can be seen, all voltages are on a stable and intended level. However, the generator and DC bus currents contains large oscillations probably due to the wide number of harmonics in the current. This is unproblematic for the simulation itself, since the controllability of the system is still given. Furthermore, reactive power consideration can be neglected in a DC bus. In real life, on the contrary, may this cause troubles with the durability of the DC-cables and capacitors, and the overshoot in current will cause additional conduction loss in cables and components. Additionally, unwanted current resonances in the grid might arise that overload the HVDC-boost converter terminal.

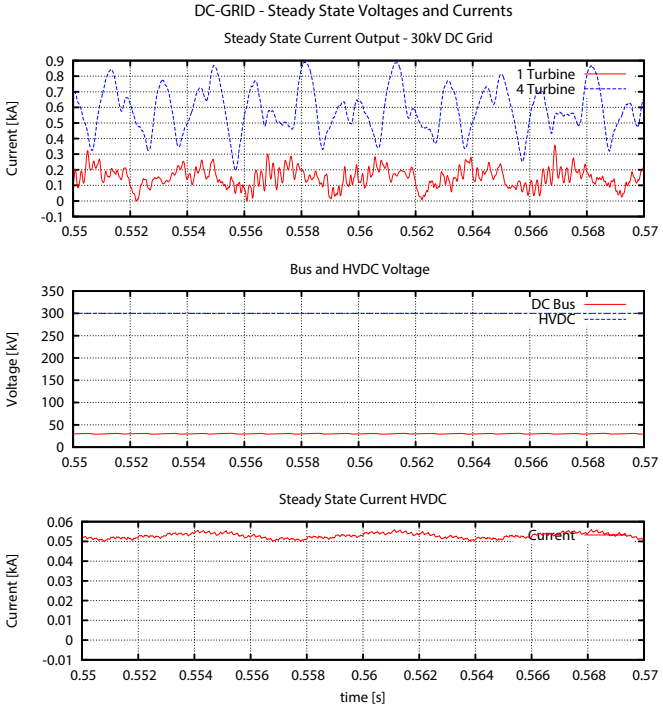

Fig. 10: Steady State Currents and Voltages

The reason for the current distortion can be explained with two factors.

The DAB converter is a topology with high input and output current ripple

Naturally, the DAB converter is a topology with a high input and output ripple (See Figure 11). This was stated from the first paper published by [5]. The control of this type of converter is utilized with fast switching square waves instead of the often used pulse width modulation. With this control approach faster switching cycles can be achieved, because no sine wave needs to be modulated. This enables the topology to reduce passive component sizes (f.x. the inductor L_1, integrated in the transformer). This is one of the main advantages of the topology.

The impedance of the grid is very low

Unlike in AC-grids, DC-grids do not contain big inductances from full scale VSC or transformers. Therefore, the grid impedance is generally very low. This implies, that changes in current will be limited only by cable and parasitic impedances in the system. Those values are naturally very low.

Both factors together create a system that delivers a very direct response to outer influences such as switching. This is one of the main differences of DC-grids compared to AC-grids and future grid designers need to pay special attention, when

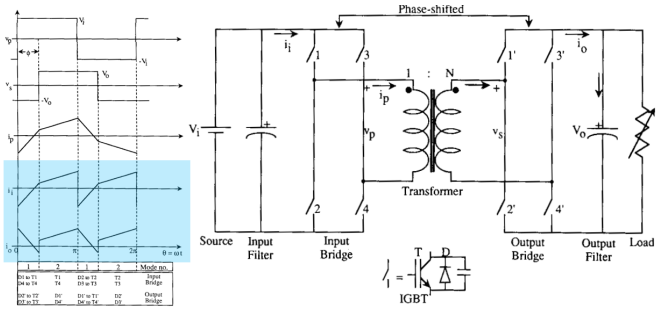

Fig. 11: Single Module of DAB - i_i=Input Current, i_o=Output Current - Blue Rectangle, Both With Huge Ripple [5]

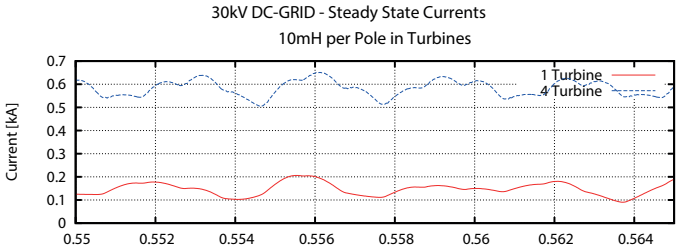

Fig. 12: Influence of Additional Inductances to the Current Output of the Turbines

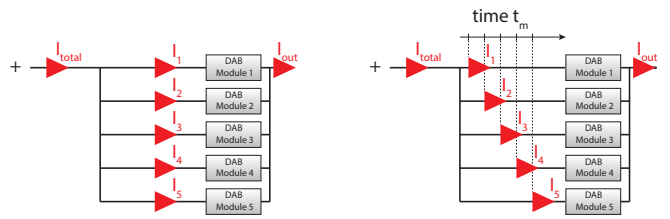

(a) Concurrent Current Flow (b) Distributed Current Flow

Fig. 13: Illustration of Concurrent and Distributed Current Inflow for DAB Converter

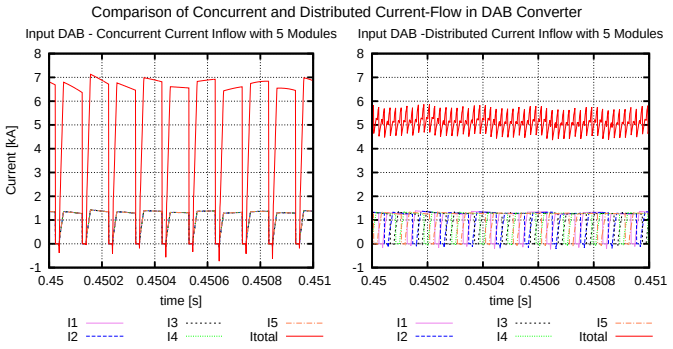

Fig. 14: Comparison of Concurrent and Distributed Current Inflow

dimensioning the first layouts. The next section introduces three approaches to limit the current distortion.

1) Reduction of ripple current with inductance: Since the impedance of the grid is very low, every switching process distorts the currents. The easiest way to prevent this behaviour is to introduce some additional inductances $L = 10mH$ on the output terminals of the DAB converters. The results of the simulations are shown in Figure 12. As can be seen, the current shapes are improved compared with the steady state results in Figure 10. If the inductor is placed close to the wind turbine terminal, the harmonic contribution of the current output for each single turbine (red graphs) is significantly reduced.

2) Reduction of ripple current with control strategy: A second possible approach to limit the switching current was observed while studying the DAB converter behaviour. This method utilizes the modular structure of the topology. In Figure 13, the input current flow of the DAB converter is illustrated. On the left hand side, the input currents of all five modules are shown in conventional operation mode. As can be seen, the current inflow happens simultaneously between all five modules. Therefore, drawn currents from all five modules will peak at the same time. The total input current I_{total} is comprised of the sum of the currents $I_1 ... I_5$. On the right hand side of Figure 13, the modules 2, 3, 4 and 5 operate with a fixed time delay t_m referred to the reference module 1. With this scheme, the current ripple in the total input current is decreased, a higher DC-offset is achieved and the peak current is reduced. The time delay between the modules can be calculated from the switching frequency of the DAB f_s, the total amount of sub modules n and the indices of the sub module m that needs to be calculated.

$$t_m = \left(\frac{1}{2fn}\right)(1-m) \tag{3}$$

Figure 14 shows the power flow in the DAB converter and the differences between the modified control strategy. This process is illustrated for the LVS of the DAB converter, however, this method can also improve the current quality of the HVS and hence improve the current quality of the DC-grid. One drawback of this approach is that the modules on the HVS can not be connected in series connection. If the modules operate with individual timings, the voltage sharing between the modules is uneven and the current flow collapses. Therefore, the modules need to be connected in parallel and the medium frequency transformers need to transform the whole voltage ratio of $\frac{30kV}{1kV}$ instead of $\frac{6kV}{1kV} * 5$.

3) Reduction of ripple current with different converter strategy: If the additional inductor option is not feasible or the reduction of ripple current is not enough, another DC/DC converter topology might be used to limit the ripple in the DC-grid. In [5], a step-up converter topology is introduce that employs a Three-Phase Dual-Active Bridge (TPDAB) converter system in the intermediate AC-circuit. Apart from the three phases, the converter topology is similar to the DAB converter and utilizes a phase shift between the bridges. Figure 15 illustrates the converter topology with in- and output waveforms. Input and output current ripple is obviously reduced compared to the DAB converter shown in Figure 11.

4) Conclusion Current Quality: For the following fault simulation of the system, the decision was made to implement

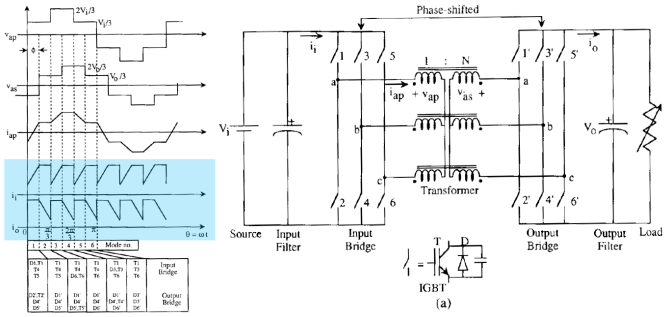

Fig. 15: Single Module of TPDAB - i_i=Input Current, i_o=Output Current - Blue Rectangle, with Reduced Ripple [5]

current filtering utilizing inductors. Additional inductors, however, will increase the impedance of the DC grid significantly and hence impact the whole fault studies in terms of resonant oscillations, voltage and current decay times (time constants) and peak magnitudes. It needs to be mentioned clearly, that the following fault scenario would look different if no inductors are added to the system. In a practical application, filter inductors will create resistive losses in the system, that could be avoided. Furthermore, the grid will become more expensive. On the other hand, reduced harmonic currents will create lower losses in cables and switches and components are not exposed to high changes of current in time $\frac{di}{dt}$. Furthermore, filter capacitor are not exposed to the ripple. This increases the durability. The fault simulations are performed with additional inductors at the turbine output terminals. The exact position of the filter inductors are marked in Figure 9.

B. Fault scenarios

Two different fault incidents are described in this study. Fault scenario 1 is directed a short circuit inside a wind turbine converter 1. Fault scenario 2 simulates a cable fault between two wind turbine 2 and 3 and the effect of a Single-Line-to-Ground fault is observed. Those incidences are assumed to represent the most common fault types in a wind farm [16]. All faults occur at simulation time $t_1 = 0.6$. Afterwards, the time to clear the fault is comprised of three contributions:

1) the time t_{detc}, the current needs to reach the critical short circuit value of this position $i_{sc_{cr}} = 5i_{steadystate}$
2) a delay for the breaker to react $t_{react} = 60\mu s$
3) the time to break the current $t_{break} = 800\mu s$

Therefore, the breaker reaction is estimated to occur around $1...1.5ms$ after the fault, depending on the rise-time of the current that will trigger t_{detc}. Breaker reaction times are found in [17].

1) Fault Scenario 1 - Converter Fault: The first scenario investigates a converter fault in a the wind turbine. A trigger for this phenomena could be dust in the converter, an insulation failure that leads to a short circuit between the phases or simply a malfunction in IGBT, snubber or gate driver. According to [16], 40% of all offshore system faults are related to converter faults. As indicated in the overview of Figure 9, the fault appears at the high voltage terminal of the DAB converter

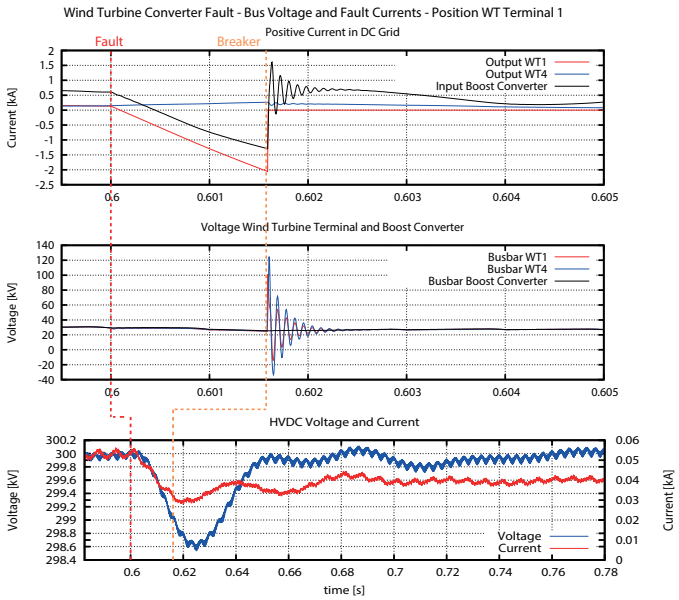

Fig. 16: Short Circuit in Wind Turbine Terminal 1

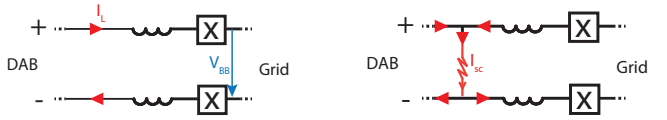

(a) Current Flow during Normal Operation

(b) Current Flow in Short Circuit Event

Fig. 17: Current Flow in Phase to Phase Terminal Faults

of turbine terminal 1. After the fault is detected, the breaker at bus bar 1 disconnects the turbine 1 from the rest of the grid.

The graphs illustrated in Figure 16 shows the behaviour of the positive phase in different positions in the grid after the fault is applied at $t = 0.6$ and cleared at $t \approx 0.6015$. The upper graph indicates the currents. During the fault, the positive currents from wind turbine 1 and the boost converter reverse the current direction and become negative. This can be explained with the sudden appearing current path through the short circuit. Figure 17 illustrates the incident. Therefore, the breaker needs to be able to operate in both the conventional and the reversed current direction. Notice that the current measurement in the simulation is performed close in the breaker. The magnitude of the negative current in the positive phase is determined by the breaker reaction time. The filter-inductor limits the current flow from the DC-grid side. As can be seen, current oscillations from the input of the boost converter appear after the breaker separated the turbine from the grid.

In Figure **??**, the voltages V_B at the different bus bars decrease slowly due to the filter inductances between the short circuit and the bus bar. After the breaker reacted and isolated the turbines, transient oscillations occur due to the sudden change of current flow. The magnitude of the DC voltage reaches $V_{BB} = 120kV$. The behaviour of the HVDC connection can be seen in the bottom part of 16. It is observable, that the voltage drops first, but stabilizes back to the reference

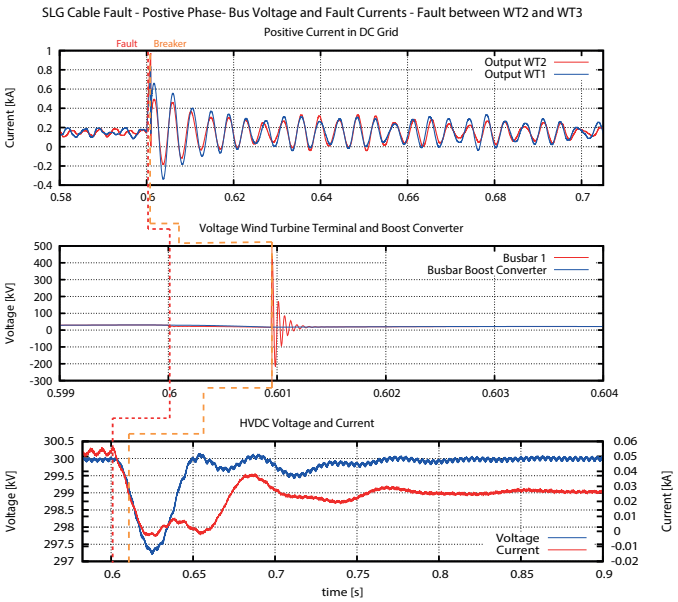

Fig. 18: Single Line to Ground Fault between Turbine 2 and 3

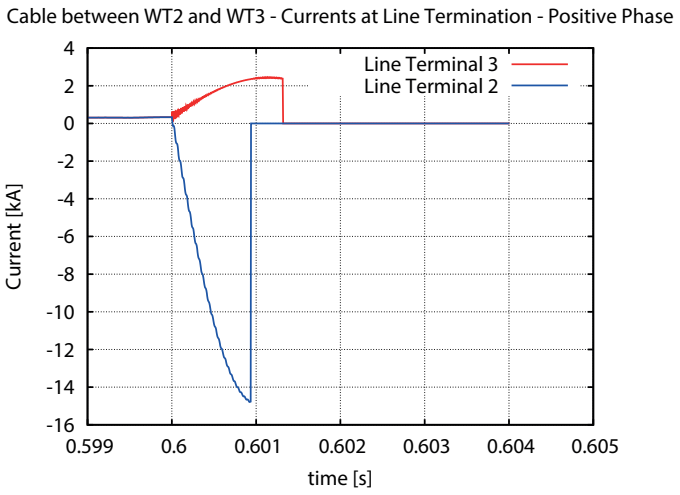

Fig. 19: Currents in the Faulty Line - Positive Phase

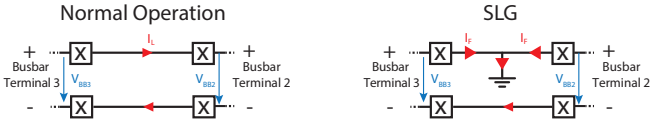

(a) Normal Current Flow in Cable between WT2 and WT3

(b) Current Flow during SLG

Fig. 20: Illustration of Fault Behaviour - SLG

voltage of $300kV$. As can be expected, the current drops after the turbine fault to around $\frac{3}{4}$ of the steady state value. Generally, it can be said, that the fault in the turbine generates high voltages and current stress for the grid. It is necessary that all components need to withstand those magnitudes for a short duration. The control system of the components is able to recover the voltages and currents after the fault to the steady state values and the wind farm can operate further.

2) Fault Scenario 2 - Cable Fault: The second fault scenario simulates a Single Line to Ground (SLG) fault in the positive phase between turbine 2 and turbine 3 (See Figure 9). This could refer to an insulation failure due to wear or ageing of the cable or a ship that inadvertently crosses the wind farm with the anchor set.

The reaction of the short-circuit in the cable is illustrated in Figure 18. The fault is applied at $t_{fault} = 0.6s$ and the breaker isolates the faulted turbines 3 and 4 at $t_{brk} \approx 0.601s$. Afterwards, distinct current oscillations with a fundamental frequency of $f_{osc} = 225Hz$ are noticeable at the output terminals of the remaining wind turbines after the fault. Furthermore, high frequency peak voltages of V_{BB_2} are detected that decay in between $t_{decay} = 0.25ms$. Afterwards, the 30 kV grid voltage is restored. Figure 19 shows the currents of the line terminals during the fault. Fault currents at line terminal 3 increases in the positive direction with a peak value of 2.4 kA. After 1.3 ms the fault is cleared. The currents from line terminal 2 reverse the current direction in case of a fault because the ground connection provides suddenly a lower potential. A schematic of the process is shown in Figure 20. The current reaches peak values up to -14.4 kA during the fault. The higher peak current can be explained with the sudden de-charge of the filter capacitor in the high voltage boost converter. The influence of the HVDC voltage and current is observable in the bottom part of Figure 18. The voltage decreases first, but stabilizes after $t = 0.2s$ at the 300 kV reference. As expected, the transmitted HVDC current is halved after the two turbines are isolated.

V. Loss Estimation

The loss estimation is conducted for the components in the MVDC grid namely: The diode bridge rectifier, the DAB converter, the filter inductor and the medium voltage cables. The HVDC boost-converter, the grid-sided HVDC inverter and the HVDC cables are not a part of the investigation since this study is directed to the medium voltage DC grid. Due to limited space, only a brief overview of the loss determination process is given. A thorough analysis of the losses is conducted in the master thesis related to this paper [18].

A. Low voltage diode rectifier

The efficiency of the diode bridge rectifier is affected by the conduction loss and the reverse recovery energy in the diodes. In the data-sheet of the diode, the forward power-loss can be determined by utilization of the average forward current I_{IFAV} through the semiconductor. I_{IFAV} can be determined with the peak current I_{peak} from the simulation for sinusoidal wave-forms:

$$I_{peak} = 6kA \tag{4}$$

Therefore,

$$I_{IFAV} = \frac{I_{peak}}{\pi} = 2kA \tag{5}$$

From Figure 21, the power loss for six diodes can be approximated with:

$$P_{L_{Diode}} = 6 * 3.2kW = 19.2kW \tag{6}$$

B. DAB converter

The loss in DAB converter is determined by following contributions: conduction loss for IGBT and anti-parallel diode, switching loss and the transformer loss. The latter is subdivided into winding loss and core loss. The switching frequency has a crucial influence for the efficiency of the converter. Conduction losses can be found with the on-state characteristics for IGBT and Diodes from the data-sheet. The switching loss is a function of the switching frequency f_s and the turn-on E_{on} and turn-off loss E_{off} in the IGBT. They can be calculated with:

$$E_{on} = E^*_{on} * \frac{V_m}{V_{base}} * \frac{I^2_m}{I^2_{base}} \tag{7}$$

and respectively

$$E_{off} = E^*_{off} * \frac{V_m}{V_{base}} * \frac{I^2_m}{I^2_{base}} \tag{8}$$

where V_m and I_m are the voltages and currents that are apparent during switching conditions , V_{base} and I_{base} are the rated conditions for the switch and E^*_{on} and E^*_{off} are the single switching energies from the data-sheet. In order to find V_m and I_m, the simulation is used to investigate the switching in steady-state full-load conditions. The power loss is then calculated with:

$$P_{sw} = (E_{on} + E_{off}) * f_s \tag{9}$$

During turn-on, the current in the DAB topology is zero and hence $E_{on} = 0$. Highest possible switching frequency is a function of the loss and the maximum handleable power-loss of the semiconductor switch ($\approx 6kW.$). The highest value for the switching frequency is $f_s = 6.2kHz$ which limits the heat to 6kW loss per switch; however, in order to avoid overloading, the switching frequency is set to $f_s = 5khZ$. The transformer loss of the DAB converter is determined with information from [8]. This recent Ph.D study presents a optimized medium-frequency transformer design with a overall efficiency of $\eta_{opt} = 0.9974$. An overview of the losses are provided in Table I.

	Type of Loss	Loss in [kW]
Transformer	Winding	13.19
	Core	8.20
	Insulation	4.900
IGBT	Conduction	27.94
	Switching	189.26
Passive Components		5.00
Total		248.49

TABLE I: Total Estimated Loss for a 5 MVA DAB Converter

C. Filter inductor

The losses of a DC smoothing inductors are determined by the flow of current through them. Following subcomponents influence the magnitude of loss: the resistance of the winding due to the DC load, the harmonics or ripple of the current, circulating currents in parallel windings, stray magnetic flux around the reactor and core losses [19]. In general, the loss of a filter reactor can be assumed to be very low, similarly to a transformer. In [20], the total shunt reactor efficiency is assumed to be $\eta_{ind} = 0.998$. If rectifier and DAB converter losses are taken into consideration, the loss of the reactor can be stated with $P_{loss} = 9.5kW$ per inductor.

Wind Turbine				Loss [kW]
		1 Turbine [kW]	4 Turbines [kW]	
Diode Rectifier		19	76	76
DAB Converter		250	1000	1000
Filter Inductor		2*10	80	80
Loss Turbines [kW]				1156
Cables				
Cable Segment	Length [km]	Current [A]	Loss (2 Conductor) [kW]	
WT1-HVDC Boost	0.85	664	27.4	27.4
WT2-WT1	0.45	498	8.2	8.2
WT3-WT2	0.45	332	3.6	3.6
WT4-WT3	0.45	166	0.9	0.9
Loss Cables [kW]			40.1	40.1
Total Loss [kW]				1196.1
Efficiency				0.9402

TABLE II: Overview of Losses in a DC grid - Full-Load Conditions

D. MV-Cables

The loss in the cables is simply determined with the resistance of the cables and the DC current in the grid. The DC current depends on the location in the grid.

$$P_L = R_{cable} * I^2_{DC} \tag{10}$$

E. Conclusion Losses

The overview of the losses is presented in Table II.

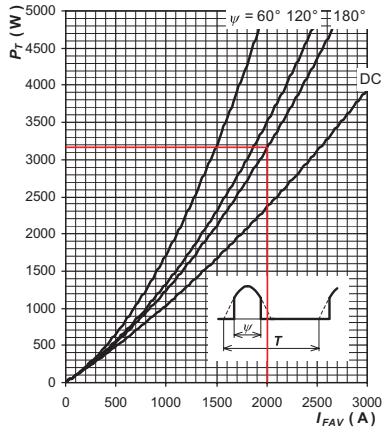

Fig. 21: Forward Power Loss vs. Average Forward Current Characteristic for Diode Power Loss Estimation

VI. Conclusion

This study investigated the operational conditions of a DC collection network for offshore wind application. The most suitable component models are identified and control strategies are evaluated and implemented. One main goal of this work was to identify suitable bidirectional DC/DC converter topologies. The most promising concepts is the Dual-Active Bridge converter. It combines high power capability, an easy control pattern, a good transient response, and the possibility to share the load between several modules. The drawback of this concept is the high input and output current ripple. After all models are selected and tested individually, the overall DC grid simulation in PSCAD/EMTDC was implemented. One parallel feeder consisting out of four wind turbines was evaluated. First, the steady-state voltages and currents were monitored. It was observed that the voltages were stable and did not possess a high ripple; however, the currents in the DC grid were full of harmonics. Two reasons are identified for this occurrence. Firstly, the grid impedance of the collection network is determined solely by the intrinsic medium voltage cables and can be estimated with a very low value. This means that, unlike in AC grids, where huge transformers characterise the grid impedance, the response to switching will be more distinct. Secondly, the high input and output ripple of the investigated DAB converter propagates the disturbance for the currents further. Three different approaches to solve the ripple current issue are proposed, and the introduction of additional inductors was an efficient method to reduce the ripple current, which is finally implemented in the PSCAD simulation. With the improved operating condition, the fault analysis was conducted. Three different approaches to solve the ripple current issue were proposed, and the introduction of additional inductors was an efficient method to reduce the ripple current, which was implemented in the PSCAD simulation in the end. In the simulation, every turbine and cable segment was protected with a set of bipolar DC breakers, each equipped with with a automated control scheme. If a certain current value was detected, the breaker reacted and isolated faulty turbines or entire cable segments. With the re-evaluated operating condition, the fault analysis was conducted. The first scenario is directed to a wind turbine converter fault and the second scenario investigates a SLG cable fault between two turbines. In case of a turbine converter fault, high current and voltage oscillations appeared but the control of the grid was able to be restore the rated voltage in $\approx 3ms$. The study of the cable fault resulted in high current oscillations, but after the fault location was isolated, the system was able to return to steady state conditions. Finally, the calculated losses for the DC grid. With the given layout, the efficiency of the network was determined to be $\eta = 94.02\%$.

Acknowledgment

The author gratefully acknowledges the support of Tonny W. Wederberg, Walid Ziad El-Khatib and Joachim Holbøll during the development process of this work. This paper wraps-up a master thesis submitted 09/2014 and a more detailed analysis about DC Collection Networks for Offshore Wind Farms can be found there [18].

References

[1] C. Meyer, M. Hoeing, A. Peterson, and R. W. De Doncker, "Control and design of dc grids for offshore wind farms," *IEEE TRANSACTIONS ON INDUSTRY APPLICATIONS*, vol. 43, no. 6, pp. 1475–1482, 2007.

[2] L. Max, *Design and control of a DC collection grid for a wind farm*, ser. Doktorsavhandlingar vid Chalmers tekniska hgskola. Ny serie, no: 3014. Institutionen fr energi och milj, Elteknik, Chalmers tekniska hgskola,, 2009, 167.

[3] J. Robinson, D. Jovcic, and G. Joos, "Analysis and design of an offshore wind farm using a mv dc grid," *IEEE TRANSACTIONS ON POWER DELIVERY*, vol. 25, no. 4, pp. 2164–2173, 2010.

[4] J. Yang, J. Fletcher, and J. O'Reilly, "Multiterminal dc wind farm collection grid internal fault analysis and protection design," *Power Delivery, IEEE Transactions on*, vol. 25, no. 4, pp. 2308–2318, Oct 2010.

[5] R. W. A. A. De Doncker, D. M. Divan, and M. H. Kheraluwala, "A three-phase soft-switched high-power-density dc/dc converter for high-power applications," *IEEE Transactions on Industry Applications*, vol. 27, no. 1, pp. 63–73, 1991.

[6] D. Jovcic, "Bidirectional, high-power dc transformer," *IEEE TRANSACTIONS ON POWER DELIVERY*, vol. 24, no. 4, pp. 2276–2283, 2009.

[7] T.Hansen, "Offshore wind farm layouts - performance comparison for a 540 mw offshore wind farm," Master's thesis, Norwegian University of Science and Technology, 2009.

[8] M. A. Bahmani, *Design and Optimization of HF Transformers for High Power DC-DC Applications*. Institutionen fr energi och milj, Elteknik, Chalmers tekniska hgskola,, 2014.

[9] G. Ortiz, J. Biela, and J. Kolar, "Optimized design of medium frequency transformers with high isolation requirements," in *IECON 2010 - 36th Annual Conference on IEEE Industrial Electronics Society*, Nov 2010, pp. 631–638.

[10] H. Bai and C. Mi, "Eliminate reactive power and increase system efficiency of isolated bidirectional dual-active-bridge dc-dc converters using novel dual-phase-shift control (vol 23, pg 2905, 2008)," *IEEE TRANSACTIONS ON POWER ELECTRONICS*, vol. 27, no. 9, pp. 4177–4177, 2012.

[11] J. Yang, J. O'Reilly, and J. E. Fletcher, "An overview of dc cable modelling for fault analysis of vsc-hvdc transmission systems," *Aupec 2010 - 20th Australasian Universities Power Engineering Conference: "power Quality for the 21st Century", Aupec - Australas. Univ. Power Eng. Conf.: "power Qual. Century"*, 2010.

[12] M. PSCAD, *PSCAD Manual - Frequency Dependent Models*, help Files regarding Frequency Dependent Models.

[13] F. Mura, C. Meyer, and R. W. De Doncker, "Stability analysis of high-power dc grids," *Conference Record - Industrial and Commercial Power Systems Technical Conference*, pp. –, 2009.

[14] *Basic Calculation of a Boost Converter's Power Stage*, Texas Instruments, http://www.ti.com/lit/an/slva372c/slva372c.pdf, 2009/2014.

[15] R. Pena, J. Clare, and G. Asher, "Doubly fed induction generator using back-to-back pwm converters and its application to variable-speed wind-energy generation," *Electric Power Applications, IEE Proceedings -*, vol. 143, no. 3, pp. 231–241, May 1996.

[16] P. Zhu, Y. Liu, R. Robert, and X. Hao, "Offshore wind converter reliability evaluation," *8th International Conference on Power Electronics - ECCE Asia: "Green World With Power Electronics", ICPE 2011-ECCE Asia*, pp. 966–971, 2011.

[17] Meyer, Kowal, and D. Doncker, "Circuit breaker concepts for future high-power dc-applications," *Conference Record, Industry Applications Society, IEEE-IAS Annual Meeting*, vol. 2, pp. 860–866 Vol. 2, 2005.

[18] W. E.-K. J. H. S. Vogel, T. Rasmussen, "Investigation of dc collection networks for offshore wind farms," Master's thesis, Technical University of Denmark, August 2014.

[19] "Ieee standard general requirements and test code for dry-type and oil-immersed smoothing reactors for dc power transmission," *IEEE Std 1277-2010 (Revision of IEEE Std 1277-2000)*, pp. 1–102, June 2010.

[20] F. M. Z. Gajic, B. Hillstrom, "Hv shunt reactor secrets for protection engineers," in *30th Western Protective Relaying Conferencen*, Oct 2003, pp. 1–30.